Advanced Hyperspectral Remote Sensing for Target Detection

Conference Paper · September 2011

DOI: 10.1109/ICSEng.2011.43 · Source: IEEE Xplore

2 authors, including:

Ershad Sharifahmadian

27 PUBLICATIONS **104** CITATIONS

SEE PROFILE

2011 21st International Conference on Systems Engineering

Advanced Hyperspectral Remote Sensing for Target Detection

Ershad Sharifahmadian
Dept. of Electrical & Computer Engineering
University of Nevada, Las Vegas, USA
sharifah@unlv.nevada.edu

Shahram Latifi
Dept. of Electrical & Computer Engineering
University of Nevada, Las Vegas, USA
Shahram.latifi@unlv.edu

***Abstract*—** Hyperspectral sensors provide 3-D images with high spatial and spectral resolution. Acquired data can be utilized in diverse applications such as detection and control of hazardous agents in atmosphere and water, military targets, and so on. Over the last decade, hyperspectral remote sensing algorithms for target detection have evolved from the spectral-based methods, which only use spectral information, to more recent methods based on spatial-spectral information. Spatial information plays a crucial role to improve the efficiency of the algorithms. Furthermore, the parallelization of the algorithms reduces the computation time. Developments in the area of commodity computing provide affordable approach for target detection applications with real-time constraint. We will give a scientific overview of recent target detection algorithms which try to overcome existing limitations (e.g. spectral variability or background interference) in hyperspectral remote sensing. Unlike current target detection methods in literature, this study explains and assesses different aspects of developments in target detection algorithms comprehensively. In particular, this study focuses on development in atmospheric correction methods which especially deal with background interference, development in methods based on spectral information and spectral-spatial information (both methods especially deal with spectral variability), and parallelization of the algorithms. With consideration of hyperspectral data challenges in real-world, an optimum approach is the adaptive algorithm based on spatial-spectral information in which their computation is performed in parallel.

Keywords- Remote sensing, Spectral analysis, GPU, Parallel processing

I. Introduction

Hyperspectral Imaging (HSI) sensors provide image data containing both spatial and spectral information which can be used to detect, identify, and characterize objects of interest in the scene. HSI extends traditional remote sensing because for any object, the amount of radiation that is reflected, absorbed, or emitted varies with wavelength resulting in a specific spectra that can be used to uniquely identify, and in some circumstances, quantify the material. In fact, high spectral resolution provided by hyperspectral imagery is used to uncover and reveal many subtle information and data sources. HSI sensors measure the radiance of the materials within every pixel area at a large number of contiguous spectral subbands, with sufficient spectral resolution to perform material identification.

The spectrum measured by the HSI sensor is the solar spectrum modified by the transmittance function of the atmosphere and the reflectance spectrum of background materials. Different materials produce different electromagnetic radiation spectra unique to their chemical and physical structure (e.g. vegetation or soil). Therefore, the spectral information contained in a HSI pixel can indicate different objects present in a scene as most pixels have multiple materials contributing to the measured spectra.

These spectral data can be used to identify spatially resolved or unresolved objects based on their spectral signatures. The atmosphere affects the measured spectra because it absorbs radiation at different wavelengths selectively, due to the presence of substances in atmosphere (e.g. water vapor or oxygen). Consequently, useful information about the reflectance spectrum of the background or target materials can be lost.

To exploit the spatial information in a scene, information embedded in the spatial arrangement of pixels in every spectral band is analyzed and morphological information is extracted. Unfortunately, variability in material composition, atmospheric propagation, and sensor noise lead to random spectral variations which can influence the apparent spatial extent and relationships of the materials in the scene. Moreover, for pixels containing unresolved objects (objects smaller than the pixel), a mixture of the object and background contributions appear in the measured spectrum of the pixel as shown in Figure 1.

Two main challenges must be overcome by each detection and identification method; i) spectral variability, and ii) background interference.

Many HSI detection methods have been developed and used in the past decade. Some algorithms for spectral-feature exploitation have been developed for selected applications but these algorithms do not exploit spatial information simultaneously [1]-[3].

As classical methods, automatic target detection and classification algorithm [4] or the RX algorithm developed by Reed and Xiaoli for anomaly detection are commonly used [5]. The automatic target detection and classification algorithm searches for a set of spectrally distinct target pixels vectors by means of the concept of orthogonal subspace projection [6]. The RX algorithm is based on the application of a specific filter named RXD filter, given by the Mahalanobis distance. The pixel purity index (PPI) is a method based on exploiting the spectral information in hyperspectral data [3]. PPI has convenient results for the image analysis in Earth science. Various target and anomaly detection methods have also been proposed in the recent literature, using different concepts such as background modeling [7], [8]. However, the lack of sufficient target information makes the development and estimation of target variability models challenging. Modeling the variability of targets and the non-Gaussian behavior of backgrounds is needed to analyze a variety of target and background data more accurately.

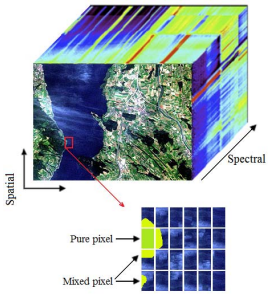

Figure 1. Pure and mixed pixels form HSI data, where a pure pixel includes a single surface material and a mixed pixel contains multiple materials.

Major causes of error in HSI data exploitation are atmospheric propagation, intrinsic spectral variability, sensor artifacts, and sensor noise. Since hyperspectral data contains absorption and scattering effects from atmospheric gases and aerosols, the

978-0-7695-4495-3 2011

DOI 10.1109/ICSEng.2011.43

atmospheric interference must be removed in order to use the hyperspectral data for target detection.

The wavelength corresponding to atmospheric water vapor is approximately 0.94 μm (but it can also be 1.14, 1.38 or 1.88 μm), the oxygen is placed in spectral band of 0.76 μm, and the carbon dioxide is placed near 2.08 μm. Thus, the half of the spectral band 0.5-2.5 μm is affected by atmospheric gas absorptions. Furthermore, the spectral bands below 1 μm is affected by molecular and aerosol scattering [9], [10].

There are three kinds of atmospheric correction methods for hyperspectral data: the scene-based empirical methods, radiative transfer modeling methods, and the hybrid approaches which is a combination of radiative modeling methods and empirical methods [11]-[15].

The scene-based empirical methods use the real remotely-sensed at-aperture radiance data in acquired hyperspectral imagery to compensate for the atmosphere; thus it is possible to utilize the exact state of the atmosphere at the time of data collection. The scene-based empirical methods need field measurements of reflectance for at least one bright object and one dark object [16].

Due to absorption by atmosphere, received spectral data is not similar to reflectance spectra of comparable materials measured in the field or laboratory [17]-[18].

In scene-based empirical methods such as the Emissive Empirical Line Method (EELM) [11] or the In-Scene Atmospheric Correction (ISAC) [12], the atmospheric compensation parameters (e.g. atmospheric transmission τ and upwelling radiance L_u) are applicable only to the atmospheric column from which they were derived. But the calculated coefficients are generally applied to the whole collected hyperspectral data. This is one of limitations for scene-based empirical methods. In fact, the variable conditions of the atmosphere over huge amount of HSI data are generally not known before HSI processing [18] and atmospheric variation is assumed to be trivial but this assumption is incorrect for larger sized data sets.

The EELM is significantly affected by temperature. Temperature variability in the given method has displayed unacceptably broad variability. Thus, accurate temperature measurements should be done.

Accurate identification and estimation of the input parameters for the correction algorithm are the major challenge in scene-based empirical methods; in other words data from any geographic location should be acquired for correct estimation of the input parameters.

In radiative transfer modeling methods, the radiative transfer equation tuned with certain atmospheric requirements is used to model the atmospheric column. The at-sensor spectral radiance signal $R(\lambda_n)$ at a sensor pixel is modeled as follows [13]:

$$R(\lambda_n) = \overbrace{\frac{A(\lambda_n)}{1-\rho_e(\lambda_n)S(\lambda_n)}}^{C(\lambda_n)}\rho(\lambda_n) + \overbrace{\frac{B(\lambda_n)\rho_e(\lambda_n)}{1-\rho_e(\lambda_n)S(\lambda_n)} + R_a(\lambda_n)}^{D(\lambda_n)} \quad (1)$$

where λ_n is the central wavelength of the *n*th spectral channel, $S(\lambda_n)$ is the spherical albedo of the atmosphere, and $R_a(\lambda_n)$ is the radiance scattered by the atmosphere without reaching the surface. $\rho(\lambda_n)$ and $\rho_e(\lambda_n)$ are the pixel surface reflectance, and an average surface reflectance for the surrounding area, respectively. $A(\lambda_n)$ and $B(\lambda_n)$ are coefficients which are sensitive to atmospheric and geometric conditions, but not on the surface. It ought to be noted that $C(\lambda_n)$ and $D(\lambda_n)$ depend only on the atmospheric quantities $A(\lambda_n)$, $B(\lambda_n)$, and $S(\lambda_n)$.

This model is one of the basic assumptions for the Fast Line-of-sight Atmospheric Analysis of Spectral Hypercubes (FLAASH) algorithm [13] which is commonly used as one of radiative transfer modeling methods. Using the FLAASH, the radiance is mapped to reflectance by finding best fit to MODTRAN parameters.

The First part of equation (1) is related to radiance from both direct solar illumination and sky-shine; this radiance is reflected from the ground pixel surface and transmits directly into the sensor. The second part of the equation is related to radiance from the surface surrounding the pixel, and this radiance is scattered by the atmosphere into the sensor. The third part is related to the radiance scattered by the atmosphere without reaching the surface. Equation $R(\lambda_n) = C(\lambda_n)\rho(\lambda_n) + D(\lambda_n)$ is a linear function and demonstrates the pixel reflectance is converted to at-sensor radiance. The spatially averaged background and the atmospheric conditions have influence on $R(\lambda_n)$.

As an advantage of radiative transfer modeling methods, correction algorithm can be applied to data collected at any geographic location (i.e. a priori knowledge is not required).

Hyperspectral image processing shows intrinsic parallelism across image pixels, across spectral bands, and even across various tasks. Therefore, hyperspectral data be can processed in a parallel structure. Moreover, a new development in the area of commodity computing is the emergence of programmable graphics processing units (GPUs) [19]-[26], which provide most of capabilities of vector processors. New development in GPU technologies provides a nearly TeraFLOP computational power on a single GPU card (e.g., the NVIDIA Tesla C2070 [27]). In addition, card manufacturers provide software packages that allow everyone to use this hardware for more than graphics generation for gaming. On the other hand, the ever-growing computational requirements of HSI applications can take advantage of the relatively low cost and compact size of the graphics processing units which suggest a convenient choice for on-board image processing at much lower costs than those introduced by other devices.

During the last decade, many methods have been proposed for different aspects involved in hyperspectral remote sensing for target detection. In this paper, we present a scientific overview of promising techniques for target detection. To do this, papers after 2010 is more emphasized. This paper is organized as follows: Section II describe recent methods for atmospheric correction, new algorithms for hyperspectral data processing in spectral domain or spatial-spectral domains. Discussion about various aspects of target detection is presented in section III. Section IV concludes the paper.

II. Hyperspectral Data Processing for Target Detection: Principles and Applications

A. Atmospheric Correction

The Atmosphere CORrection Now (ACORN) [28] is one of atmospheric correction algorithms for retrieving surface reflectance from HSI data. This algorithm uses MODTRAN4 code [29] and a spectral fitting approach to model the overlap of absorption bands between liquid water in land surface and water vapor in the atmosphere.

Air Force Phillips Laboratory introduced the atmospheric correction software package called FLAASH. The FLAASH like

ACORN uses MODTRAN4 code. This algorithm corrects light scattered from adjacent pixels into the field of view [13], [30].

Two physics-based approaches of accounting for the illumination and atmospheric effects (atmospheric compensation and forward modeling) have been considered for target detection in [31]-[32]. Based on presented experiments, necessary processing steps, the computational complexity, and the flexibility related to an imperfect knowledge of acquisition conditions are assessed. It is claimed that atmospheric compensation is recommended when accurate knowledge of the acquisition conditions is available, and the collected image has relatively uniform illumination and non-shadowed targets. Moreover, the forward modeling is recommended if scene conditions are not obvious. The forward modeling is also suggested when the targets may be subject to varying illumination conditions.

The 3-Dimensional radiative transfer (RT) in the Earth-atmosphere system can be simulated by DART (Discrete Anisotropic Radiative Transfer) model [33]. DART performs in visible spectrum (from the ultra-violet band through the infrared band). This model produces 3-D spectral remote sensing images. In fact, the DART model is utilized to provide accurate simulations of HSI data with low computation time. It is claimed that the proposed method relies on a certain atmosphere grid with the use of atmosphere transfer functions for reduction of computation time, and the accuracy of the method can compete with MODTRAN-based model [34].

Accurate retrievals of water leaving reflectances should be performed to estimate chlorophyll concentrations and suspended object in the ocean. Most of atmospheric correction algorithms have acceptable results over clear ocean areas. However, most of the correction algorithms may not perform well over turbid waters because turbid waters are not dark enough for the two atmospheric correction bands (bands centered near 0.75 and 0.86 μm). Moreover, the ocean color bands saturate over bright coastal waters (bands centered near 0.488, 0.531, and 0.551 μm).

A multi-channel atmospheric correction method for remote sensing of coastal waters has been developed in [35]-[36] to give reasonable results over turbid waters and shallow waters with bottom reflection. In the proposed method, aerosol models and optical depths are defined by a spectrum-matching approach utilizing spectral bands placed at wavelengths longer than 0.86 μm where the ocean surface is dark. The aerosol information located in the visible spectrum is extracted by the derived aerosol models and optical depths. Water-leaving radiances in the visible spectrum are calculated by subtracting out the atmospheric path radiances from the satellite-measured total radiances.

B. Spatial-Spectral Methods

The spectral angle distance (*SAD*) between two pixel vectors x_i and x_j, is defined by the following expression [37]:

$$SAD(x_i, x_j) = \cos^{-1}\left(\frac{x_i . x_j}{\|x_i\|_2 . \|x_j\|_2}\right) \quad (2)$$

where x_i and x_j are two pixel vectors, and the 2-norm for pixel vector x_i, is denoted by $\|x_i\|_2$. A morphological endmember extraction algorithm has been proposed in [38] which is based on extended morphological operations and the application of morphological operations to integrate both spatial and spectral data. In fact, the impact of different vector ordering strategies on the definition of multichannel morphological operations for spectral unmixing of HSI data has been assessed. It is claimed that a strategy based on spectral angle distances between full spectral signatures provides higher quality endmembers and fractional abundance estimations than other classic methods that only use spectral information for the unmixing process.

A spatial-spectral preprocessing method for volume-based endmember extraction algorithms has been proposed in [39].

In the proposed method, spectrally pure and spatially homogeneous areas are searched by a hybrid approach that combines unsupervised clustering and volume-based concepts. A set of representative areas is then selected. This preprocessing technique is followed by a volume-based endmember extraction process using the pixels placed in such areas, which selects only a representative endmember per area. Their experimental results show spatial information can assist in the selection of spectral endmembers which are more relevant in spatial data and decrease the computation time.

In [40], an algorithm for spatial-spectral endmember extraction has been introduced to incorporate texture features in the quantification of spatial information. Their results indicate that textural information can assist in the selection of spectral endmembers. However, there is not a certain approach for combination of the final set of endmember candidates obtained by merging the individual sets of candidates found using spectral, textural and joint spectral–textural information. In fact, it is difficult to select the best possible final endmember instances out of the full set of available candidates.

The usage of the watershed transformation to integrate spatial and spectral information for endmember extraction has been introduced in [41]. The proposed method is considered as a preprocessing step to automatically select a small subset of pixels including potentially relevant candidates from both spatial and spectral domain. Using the morphological watershed transformation, it is possible to guide the endmember exploring procedure to spatially homogeneous and spectrally pure regions. Searching process for endmember extraction is to exploit the spatial similarity between adjacent pixels by defining a criterion which is sensitive to the nature of both homogenous and transition regions between different land-cover classes. The transition regions between two or more different land-cover classes could include some mixed pixels. Therefore, it is assumed that pure pixels are less likely to be found in such transition regions.

C. Spectral-Based Methods

Virtual dimensionality (VD) is one of approaches for estimation of the number of spectrally distinct signatures present in HSI data. An orthogonal subspace projection (OSP) method to estimate the VD has been introduced in [42]. In this method, linear spectral mixture analysis is considered and data sample vectors are modeled as a linear mixture of a finite set (i.e. virtual endmembers). It is claimed that the proposed method contains the SSE/HySime as its special case (i.e. the Signal Subspace Estimate, SSE, which was later improved by Hyperspectral Signal subspace Identification by Minimum Error, HySime, where the minimum mean squared error is used as a criterion to determine the VD [43]-[45]). Based on linear spectral mixture analysis, the VD can be abstracted as the minimal number of signatures which best represent the data sample vectors in a linear mixing structure.

A Gaussian noise assumption is considered in the SSE/HySime and estimation of noise covariance matrix is done by different estimation approaches. Therefore, a different noise estimation

approach may lead to a different value of the VD. Moreover, the SSE/HySime generates a single value of the VD, and the generated value does not depend on the methods used to produce signal sources. According to the results in [42], it seems the OSP methods are more flexible than the SSE/HySime in real practical applications.

In [46]-[47] spectral libraries are used to solve the hyperspectral unmixing problem. The endmembers can be derived from a large spectral library and used for unmixing applications. Moreover, results of the unmixing procedure do not depend on the availability of pure pixels in the original HSI data nor on the ability of an endmember extraction method to identify given endmembers. In the proposed approach, the sensitivity of sparse unmixing methods to certain features of real and synthetic spectral libraries, including parameters such as mutual coherence and spectral similarity between the signatures contained in the library are analyzed. Their results show improvements in the sparse unmixing algorithms in noisy environments due to pruning the libraries (by enforcing a minimum spectral angle between the signatures). However, the mutual coherence of real libraries is decreased.

Processing devices with smaller size, more flexibility, lower cost, on-board processing, and high computational power for the application of target detection are of interest. To combine the flexibility of typical microprocessors with the performance of application-specific integrated circuits, Field Programmable Gate Array (FPGA) is a promising candidate. FPGA implementation of the pixel purity index algorithm has been presented in [48]-[49] (implemented on a Virtex-II PRO XC2VP30 and on a Virtex-4 XC4VFX60 FPGAs). It is claimed that the hardware version of the PPI algorithm can improve the results in comparison with an equivalent software version of the algorithm and more accurate pure spectral extraction is provided.

The Robust Matched Filter (RMF) addresses robustness to target signature errors based on definition of an uncertainty area constraint into the optimization process [50]-[51]. The theory of Robust Capon Beamformer (RCB) [52] plays an important role in the RMF. If the mismatch is bounded by ε, then

$$\left\| s - s_0 \right\|^2 \le \varepsilon, \quad \varepsilon > 0 \tag{3}$$

where s and s_0 are actual target signature and assumed target signature, respectively. The following optimization problem is defined:

$$\min_s s^T \sum^{-1} s \quad subject \quad to \qquad \left\| s - s_0 \right\|^2 \le \varepsilon \tag{4}$$

The solution to the given optimization problem leads to a vector with diagonal loading of the covariance matrix (H_α is applied on the HSI data [53], and background clutter is related to covariance matrix)

$$H_\alpha = \frac{(\Sigma + \alpha^{-1} I)^{-1} s_0}{s_0^T (\Sigma + \alpha^{-1} I)^{-1} \Sigma (\Sigma + \alpha^{-1} I)^{-1} s_0} \tag{5}$$

The loading factor α^{-1} is obtained using the following nonlinear equation [52]

$$s_0^T (I + \alpha\Sigma)^{-2} s_0 = \sum_{n=1}^{N} \frac{\left| \tilde{s}_n \right|^2}{(1 + \alpha\lambda_n)^2} = \varepsilon \tag{6}$$

where λ_n and $\tilde{s}_n = V^T s_0$ are obtained from the Eigen-decomposition

$$\Sigma = V \Lambda V^T = \sum_{n=1}^{N} \lambda_n v_n v_n^T \tag{7}$$

D. Parallel Processing

Graphics processing units can be abstracted as a data set model, under which all data sets are defined as Ordered Data Sets (ODS). Different kernels are utilized for parallelism, and apply on entire ODS. These kernels take one or more ODS as inputs and generate one or more ODS as outputs. GPU architectures follow two main steps: First, a data set of vertices from a 3-dimensional polygonal mesh is considered. Vertex processors convert the 3-dimensional data of every vertex of the given mesh into a 2-dimensional screen position, and use lighting to identify their colors. In the second step, the converted vertices are first categorized into rendering primitives and scan-converted into a data set of pixel fragments. The fragments are discrete partitions of the surface related to the pixels of the rendered image. Interpolation of attributes stored at the vertices is also performed and the interpolated values are stored at every fragment. Afterwards, some operations and texture lookups are done by processors to identify the color for the fragment. In fact, to map non-graphics methods onto GPUs, the HSI data should be arranged as ordered data sets (ODS is considered as textures).

The first issue that needs to be addressed is how to map a HSI data onto the memory of the GPU. As the size of HSI data significantly exceeds the capacity of GPU memory, HSI data should be split into multiple spatial-domain blocks (Figure 2).

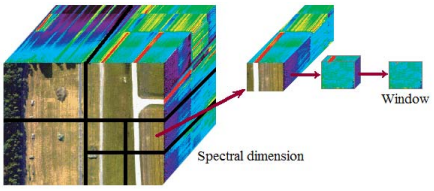

Figure 2. Window is extracted during spatial decomposition

Every spatial-domain block is further split into small blocks, and each small block is split into windows which are then divided into tiles. Tiles from four consecutive spectral bands are then arranged and mapped onto the RGBA color channels of a texture element in GPU. When the HSI data is mapped onto the GPU memory, a grid is created, and all pixels in the input data are processed in parallel.

In [54], parallel implementations of a target detection algorithm have been proposed based on orthogonal subspace projections. The parallel versions are tested by a parallel cluster of computers called Thunderhead and a commodity graphics processing unit (GPU) of NVidia GeForce GTX 275 type. The GPU implementation is performed near real-time anomaly detection in HSI data, with speed ups over 50x in comparison with a highly optimized serial implementation [54]. Their assessment of clusters versus GPUs (based on used dataset) explains that commodity clusters show a source of computational power which is both accessible and applicable to reach results quickly enough and with high reliability in target detection applications in which the data has already been transmitted to Earth. However, GPU implementation can be used for cases in which a real-time response is of interest.

The GPU implementation of PPI method has been explained in [55] and implemented using the compute device unified architecture (CUDA), and tested on the NVidia Tesla C1060 architecture.

In [56], a GPU-based implementation of the N-FINDR algorithm has been introduced. Winter's N-FINDR algorithm [55] is one of the successfully applied methods for endmember extraction directly from the input HSI data. The proposed work is quantitatively assessed based on endmember extraction accuracy and parallel efficiency, using two different generations of GPUs from NVidia.

The parallel implementation of automatic target detection and classification algorithm (ATDCA) and RX algorithm have been presented in [57]-[58]. The parallel performance of the proposed methods is assessed using an NVidia GeForce 9800 GX2 GPU.

Linear spectral unmixing is considered as a standard technique for spectral mixture analysis. In this technique, the acquired HSI data is expressed in the form of a linear combination of endmembers weighted by their corresponding abundances, with two constraints; all abundances should not be negative, and the sum of abundances for a given pixel should be unity. Various techniques have been proposed in the literature for unconstrained, partially constrained and fully constrained linear spectral unmixing. The complex high-dimensional data with a high number of endmembers should be processed but it is computationally expensive. In [59], GPU implementations of unconstrained, partially constrained and fully constrained abundance estimation algorithms have been introduced. The proposed approaches are tested on the NVidia Tesla C1060 architecture.

III. Discussion

Target detection algorithms can be evaluated based on various criteria. However, robust detection with the lowest number of false alarm is always sought. Anomaly detectors produce too many false alarms for most practical applications. Real-time applications are making this situation even worse.

Target detection algorithms need better selectivity among spectral bands to decrease the number of false alarms. Using signature library and spatial information, it is possible to reduce the number of false alarm.

Moreover, accurate atmospheric correction methods should be developed. For scene-based empirical methods, it is very difficult to achieve excellent absolute calibration but the methods are computationally simple and generally work well. The radiative transfer modeling methods are sufficiently mature and can be utilized for routine analysis of HSI data. As mentioned in section I, these methods can be applied on data acquired at any geographic location.

Despite the growing interest in parallel processing of HSI data, only a few parallel implementations for target detection exist in the open literature [60]. However, due to the computational complexity of HSI algorithm and high dimensionality of HSI data, parallel processing is expected to be necessary for target detection applications. Furthermore, some applications require near real-time processing performance.

An initial step in parallel Implementation of a target detection algorithm (Implementation into clusters, FPGAs or GPUs) is data partitioning; Partitioning can be done in spectral domain or spatial domain depending on the algorithm. For spectral-domain partitioning, a spectral signature may be stored in different processors and communications would be necessary for individual signature-based computations (e.g. spectral angle distance). For spatial-domain partitioning, each spectral signature is stored in the same processor.

Recently, GPUs are emerged as a low-cost specialized hardware for on-board processing. GPUs provide significant speedups at low cost.

Parallel implementation of target detection algorithms can be performed using clusters, FPGAs, or GPUs. Here, some features related to each implementation are explained.

i) Clusters: its adaptation for on-board processing is difficult; convenient choice for information extraction from repositories of HSI data transmitted to Earth; power consumption is challenging; large number of processors is required for real-time response; high maintenance and space are required.

ii) FPGAs: convenient choice for on-board processing because of light weight and low power consumption; reconfigurable hardware; real-time response could not be obtained without occupying most resources.

iii) GPUs: It can be used for real-time applications with low cost; low-weight but demanding from a power consumption point of view.

In fact, parallel implementation of target detection algorithms by GPUs could be simpler than the implementation by FPGAs because the board should be designed for the FPGA implementation but the device is only used in the GPU implementation. Moreover, one of challenging issues in large FPGA design is debugging hardware.

IV. Conclusion

In real-world, applications of HSI algorithms have to consider many issues which are generally overlooked. For instance, finding a threshold to maintain a constant false-alarm rate is difficult. Some other practical obstacles are atmospheric compensation, sensor noise, sensor calibration, a few number of pixels in comparison with the number of spectral bands, background variations, and in particular target mismatch. These obstacles force that any small performance gain provided by complicated detectors can be irrelevant in practical applications, where the aim is to reach the best performance while the least amount of a priori knowledge is necessary.

Moreover, a large number of HSI detection algorithms in literature are evaluated by specific datasets or simulated data. Although their results could be promising but no one can explicitly say one method is the best due to the difficulty of data acquisition with a variety of targets and insufficient number of pixels per target. In conclusion, with consideration of hyperspectral imaging challenges in real-world, adaptive detection algorithms with high computational tractability and robust behavior are of interest. In fact, an optimum approach can be the GPU-based algorithm which is the combination of an enhanced version of robust matched filter and morphological endmember extraction algorithm.

Acknowledgment

This work was conducted as a part of an Innovation Working Group supported by the Nevada EPSCoR Programs, and funded by NSF Grant # NSF- EPS-0814372.

References

[1] N. Keshava and J. F. Mustard, "Spectral unmixing," *IEEE Signal Processing Mag*., Vol. 19, Jan. pp. 44–57, 2002.

[2] M.E. Winter, "N-FINDR: An algorithm for fast autonomous spectral end-member determination in hyperspectral data," *Proc. SPIE*, Vol. 3753, pp. 266-275, 1999.

[3] J.W. Boardman, et. al "Mapping target signatures via partial unmixing of AVIRIS data," *VI JPL AVIRIS Workshop*, CA, 1995.

[4] H. Ren, "Automatic spectral target recognition in hyperspectral imagery," *IEEE Trans. Aerosp. Syst*., pp.1232–1249, 2003.

[5] I. Reed and X. Yu, "Adaptive multiple-band cfar detection of an optical pattern with unknown spectral distribution," *IEEE Trans. Acou. Speech and Sig. Proc.*, Vol. 38, pp. 1760–1770, 1990.
[6] J. C. Harsanyi, et. al, "Hyperspectral image classification and dimensionality reduction: An orthogonal subspace projection approach," *IEEE Trans. Geos. Rem. Sens*., pp.779–785, 1994.
[7] J.B. Adams, et. al "Imaging Spectroscopy: Interpretation Based on Spectral Mixture Analysis," *chap. 7 in Remote Geochemical Analysis,* Cambridge Press, pp.145–166, 1993.
[8] W.J. Stein, et. al "Anomaly Detection from Hyperspectral Imagery," *IEEE Signal Process. Mag*., Vol. 19, pp. 58–69, 2002.
[9] A. Goetz, et. al "Imaging spectrometry for Earth remote sensing," *Science*, No. 228, pp.1147–1153, 1985.
[10] G. Vane, et. al, "The Airborne Visible/Infrared Imaging Spectrometer," *Remote Sens. Env*., No. 44, pp.127-143, 1993.
[11] A. R. Gillespie, "Lithologic mapping of silicate rocks using TIMS," *The TIMS Data User's Workshop*. JPL, pp. 29-44, 1985.
[12] S. Young, et. al "An in-scene method for atmospheric compensation of thermal hyperspectral data," *Jour. Geophysical Research*, Vol. 107, 2002.
[13] S. Golden-Adler, et al., "FLAASH, A MODTRAN4 atmospheric correction package for hyperspectral data retrievals and simulations," No. 97-21, JPL, 1998.
[14] M. Matthew, et. al "Atmospheric correction of spectral imagery: Evaluation of the FLAASH algorithm with AVIRIS data," *SPIE*: *Algorithms and Technologies for Multispectral, Hyperspectral and Ultraspectral Imagery IX*, Vol. 5093, 2003.
[15] R. N. Clark, et. Al "Calibration of surface reflectance of terrestrial imaging spectrometry data: Comparison of methods," *5th Annual JPL Workshop*, JPL Publication 95-1,pp. 41- 42, 1995.
[16] J. E. Conel, et. al, "AIS-2 radiometry and a comparison of methods for the recovery of ground reflectance," *JPL Workshop*, pp. 18-47, 1987.
[17] R. N. Clark, et. al, "Causes of spurious features in spectral reflectance data," JPL *Workshop*, pp. 49-61, 1987.
[18] B. C. Gao, et. al "A Review of Atmospheric Correction Techniques for Hyperspectral Remote Sensing of Land Surfaces and Ocean Color," IEEE *Geosc. and Remote Sensing Sym.*, July 31-Aug. 4, pp.1979-1981, 2006.
[19] A. Plaza, et. al, "Parallel Implementation of Endmember Extraction Algorithms Using NVidia Graphical Processing Units," *IEEE Inter. Geosc. and Remote Sensing Sym.*, Cape Town, South Africa, 2009.
[20] J. Li, et. al "On robust capon beamforming and diagonal loading," *IEEE Trans. on Signal Processing*, Vol. 51, No. 7, pp. 1702 – 1715, 2003.
[21] J. Setoain, et. al "Parallel morphological endmember extraction using commodity graphics hardware," *Geosci. Remote Sens.*, pp.441–445, 2007.
[22] A. Plaza, et. al, "Clusters versus FPGA for Parallel Processing of Hyperspectral Imagery," *High Performance Com. App.*, pp.366-385, 2008.
[23] A. Plaza, "Recent Developments and Future Directions in Parallel Processing of Remotely Sensed Images," *6th IEEE ISISPA*, Austria, 2009.
[24] A. Plaza, et. al, "Optimizing a Hyperspectral Image Processing Chain Using Heterogeneous and GPU-Based Parallel Computing Architectures," *Computational and Mathematical Methods in Sci. and Eng.*, Spain, 2009.
[25] J. Setoain, et. Al "GPU for Parallel On-Board Hyperspectral Image Processing," *High Performance Comput. Applications*, pp.424–437, 2008.
[26] A. Plaza, et. al "Improving the Performance of Hyperspectral Image and Signal Processing Algorithms Using Parallel, Distributed and Specialized Hardware-Based Systems," *Sig. Proc. Sys.*, pp. 293-315, 2010.
[27] http:// www.nvidia.com/tesla
[28] A. F. Kruse, "Comparison of ATREM, ACORN, and FLAASH atmospheric corrections using low-altitude AVIRIS data of Boulder," *CO. Summaries of 13th JPL Workshop*, Jet Propulsion Lab, Pasadena, CA, 2004.
[29] A. Berk, et. al, "MODTRAN: a moderate resolution model for LOWTRAN7," GL-TR-89-0122, AFGL, Hanscom AFB, 1989.
[30] B. C. Gao, et. al, "Atmospheric correction algorithms for hyperspectral remote sensing data of land and ocean," *Elsevier*, pp. S17-S24, 2009.
[31] S. Matteoli, et. al "Operational and Performance Considerations of Radiative-Transfer Modeling in Hyperspectral Target Detection," *IEEE Trans. on Geoscience and Remote Sensing*, No.99, Oct. 2010.
[32] S. Matteoli, et. Al "Forward Modeling and Atmospheric Compensation in hyperspectral data: Experimental analysis from a target detection perspective," *1st Workshop on HISP*, Aug. 2009.
[33] E. Grau, et. Al "Earth-Atmosphere radiative transfer in DART model," *1st Workshop on HISP*, Aug. 2009.
[34] G. Healey "Models and methods for automated material identification in hyperspectral imagery acquired under unknown illumination and atmospheric conditions," *IEEE Trans. on Geosc. and Remote Sensing*, vol. 37, no. 6, pp. 2706–2717, Nov. 1999.
[35] B. C. Gao, et. al "A multi-channel atmospheric correction algorithm for remote sensing of coastal waters," *IEEE Geosc. Sym.*, 2007.
[36] B. C. Gao, et. al, "An Atmospheric Correction Algorithm for Remote Sensing of Bright Coastal Waters Using MODIS Land and Ocean Channels in the Solar Spectral Region," *IEEE Trans. on Geosci.,* June 2007.
[37] C. I. Chang, "Hyperspectral Imaging: Techniques for Spectral Detection and Classification," Norwell, MA: Kluwer, 2003.
[38] A. Plaza, "Impact of Vector Ordering Strategies on Morphological Unmixing of Remotely Sensed Hyperspectral Images," *20th International Conference on Pattern Recognition*, Istanbul, Turkey, 2010.
[39] G. Martin, "Spatial-Spectral Preprocessing for Volume-Based Endmember Extraction Algorithms Using Unsupervised Clustering," *IEEE GRSS Workshop on HISP*, Reykjavik, Iceland, 2010.
[40] M. Zortea, et. al, "Spectral-Textural Endmember Extraction," *IEEE GRSS Workshop on HISP*, Reykjavik, Iceland, 2010.
[41] M. Zortea, and A. Plaza, "Spatial-Spectral Endmember Extraction from Remotely Sensed Hyperspectral Images Using the Watershed Transform," *IEEE Geosc. and Remote Sensing Sym.*, Hawaii, USA, 2010.
[42] C. I. Chang, et. al "Linear Spectral Mixture Analysis Based Approaches to Estimation of Virtual Dimensionality in Hyperspectral Imagery," *IEEE Trans. on Geosc. and Remote Sens.*, pp. 3960-3979, 2010.
[43] J. M. Bioucas-Dias, "Hyperspectral subspace identification," *IEEE Trans. Geosci. Remote Sens*., Vol. 46, No. 8, pp. 2435–2445, Aug. 2008.
[44] J. M. Bioucas-Dias, "Estimation of signal subspace on hyperspectral data," *Proc. SPIE*, Vol. 5982, Bruges, Belgium, pp. 191–198, Sept. 2005.
[45] J. W. Boardman, "Geometric mixture analysis of imaging spectrometry data," *Int. Geosci. Remote Sens. Symp*., pp. 2369–2371, 1994.
[46] M. D. Iordache, et. Al "On the Use of Spectral Libraries to Perform Sparse Unmixing of Hyperspectral Data," *IEEE GRSS HISP*, Iceland, 2010.
[47] M. D. Iordache, et. al, "Sparse Unmixing of Hyperspectral Data," *IEEE Trans. on Geosci. and Remote Sensing*, 2010.
[48] C. Gonzalez, "FPGA for Computing the Pixel Purity Index Algorithm on Hyperspectral Images," *Eng. of Reconfigurable Sys.,* Las Vegas, 2010.
[49] C. Gonzalez, et. al "FPGA Implementation of the Pixel Purity Index Algorithm for Remotely Sensed Hyperspectral Image Analysis," *EURASIP Journal on Advances in Signal Proc.*, vol. 2010, Article ID 969806, 2010.
[50] D. Manolakis, et. al, "Hyperspectral detection algorithms: Use covariances or subspaces?" *SPIE Annu. Meeting*, Vol.7457, CA, 2009.
[51] D. Manolakis, et. al "Effects of Signature Mismatch on hyperspectral Detection Algorithms," *2nd Workshop on HISP*, pp.1-4, 2010.
[52] J. Li, et. al, "On robust capon beamforming and diagonal loading," *IEEE Trans. on Signal Proc.*, Vol. 51, No. 7, pp. 1702 – 1715, 2003.
[53] D. Manolakis, "Hyperspectral Image Processing for Automatic Target Detection Applications," *Lincoln Lab. Jour*., Vol. 14, pp.79-116, 2003.
[54] A. Paz, and A. Plaza, "Cluster versus GPU Implementation of an Orthogonal Target Detection Algorithm for Remotely Sensed Hyperspectral Images," *IEEE Conf. on Cluster Computing*, Greece, 2010.
[55] S. Sanchez and A. Plaza, "GPU Implementation of the Pixel Purity Index Algorithm for Hyperspectral Image Analysis," *IEEE ICCC*, 2010.
[56] S. Sanchez, et. al, "Parallel Implementation of the N-FINDR Endmember Extraction Algorithm on Commodity Graphics Processing Units," *IEEE Inter. Geosci. and Remote Sensing Sym.*, Hawaii, USA, 2010.
[57] A. Paz and A. Plaza, "GPU Implementation of Target and Anomaly Detection Algorithms for Remotely Sensed Hyperspectral Image Analysis," *SPIE Optics and Photonics,* San Diego, CA, 2010.
[58] A. Paz, and A. Plaza, "Clusters versus GPUs for Parallel Automatic Target Detection in Remotely Sensed Hyperspectral Images," *EURASIP Journal on Advances in Signal Proc.*, vol. 2010, Article ID 915639, 2010.
[59] S. Sanchez, et. al "GPU Implementation of Fully Constrained Linear Spectral Unmixing for Remotely Sensed Hyperspectral Data Exploitation," *SPIE Optics and Photonics,* San Diego, CA, 2010.
[60] A. Paz, A. Plaza, and S. Blazquez, "Parallel implementation of target and anomaly detection algorithms for hyperspectral imagery," *Proc. IEEE Geosci. Remote Sens. Symp*., vol. 2, pp. 589–592, 2008.